

Cosmochim. Acta **41**, 1145 (1977); T. E. Bunch and S. Chang, *ibid.* **44**, 1543 (1980); G. P. Meeker, G. J. Wasserburg, J. T. Armstrong, *ibid.* **47**, 707 (1983); M. E. Zolensky, W. C. Bourcier, J. L. Gooding, *Icarus* **78**, 411 (1989).

10. D. E. Brownlee et al., *Lunar Planet. Sci. Conf. XXIV*, 205 (1993); D. E. Brownlee et al., *ibid.* **XXV**, 185 (1994).

11. M. V. Sykes, L. A. Lebofsky, D. M. Hunten, F. Low, *Science* **232**, 1115 (1986); J. P. Bradley and D. E. Brownlee, *ibid.* **251**, 549 (1991); A. A. Jackson and H. A. Zook, *Icarus* **97**, 70 (1992).

12. IDPs are collected in the stratosphere at an altitude of 20 to 25 km by NASA U2 and RB57 aircraft. See D. E. Brownlee, *Annu. Rev. Earth Planet. Sci.* **13**, 147 (1985); S. A. Sandford, *Fundam. Cosmic Phys.* **12**, 1 (1987).

13. J. M. Greenberg, in *Comets*, L. L. Wilkening, Ed. (Univ. of Arizona Press, Tucson, 1982), p. 131; F. L. Whipple, in *The Zodiacal Light and the Interplanetary Medium*, J. L. Weinberg, Ed. (Office of Technology Utilization, NASA, Washington, DC, 1967), pp. 409-426; J. S. Dohnanyi, in *Cosmic Dust*, J. A. M. McDonnell, Ed. (Wiley-Interscience, New York, 1978), pp. 527-605; M. S. Hanner, J. A. Hackwell, R. W. Russel, D. K. Lynch, *Icarus*, in press.

14. E. Anders and M. Ebihara, *Geochim. Cosmochim. Acta* **46**, 2363 (1984).

15. At least three classes of IDPs with approximately chondritic (solar) bulk compositions are recognized [see S. A. Sandford and R. M. Walker, *Astrophys. J.* **291**, 838 (1985); J. P. Bradley, *Geochim. Cosmochim. Acta* **52**, 889 (1988)]. The IDPs reported here belong to the anhydrous "chondritic porous" (CP), typically pyroxene-rich but some with significant amounts of olivine (L. S. Schramm, M. M. Wheelock, D. E. Brownlee, *Meteoritics* **24**, 99 (1989)). Most identified cometary IDPs belong to the CP class (10). Isotopic anomalies have been found in 13 IDPs, about 40% of the particles so far studied; D/H enrichments (associated with C) and ¹⁵N enrichments suggest the survival of an organic component from cold interstellar clouds [see K. D. McKeegan, R. M. Walker, E. Zinner, *Geochim. Cosmochim. Acta* **49**, 1971 (1985); F. J. Stadermann, R. M. Walker, E. Zinner, *Meteoritics* **24**, 327 (1989)]. Enrichments of D and ¹⁵N have also been found in meteorites, but anomalies in C, O, Mg, and Si that are found in meteorites have yet to be found in chondritic IDPs. The small sizes of IDPs and their extreme submicrometer-scale heterogeneity complicate detection of isotope anomalies.

16. J. P. Bradley, S. A. Sandford, R. M. Walker, in (6), p. 861.

17. J. P. Bradley and D. E. Brownlee, *Science* **231**, 1542 (1986).

18. J. P. Bradley, *Geochim. Cosmochim. Acta* **58**, 2123 (1994).

19. F. J. M. Rietmeijer, *Proc. Lunar Planet. Sci. Conf.* **19**, 513 (1989); in *Analysis of Interplanetary Dust*, M. E. Zolensky, F. J. M. Rietmeijer, G. J. Flynn, Eds. (American Institute of Physics, New York, 1994), p. 231.

20. J. P. Bradley, H. J. Humecki, M. S. Germani, *Astrophys. J.* **394**, 643 (1992).

21. J. P. Bradley, *Geochim. Cosmochim. Acta* **52**, 889 (1988).

22. Data were acquired with the use of a 200-keV JEOL (Peabody, MA) 2010 AEM equipped with a Noran TN5500 x-ray EDS sensitive to elements with atomic number Z > 5, and a Gatan (parallel detection) electron energy-loss spectrometer. A thin-film procedure was used in measuring the compositions [see G. Cliff and G. W. Lorimer, *J. Microsc.* **103**, 203 (1975)]. Experimental EDS correction (K) factors were derived from analyses of thin-film standards [see J. P. Bradley, M. S. Germani, D. E. Brownlee, *Earth Planet. Sci. Lett.* **93**, 1 (1989); M. S. Germani, J. P. Bradley, D. E. Brownlee, *ibid.* **101**, 162 (1990)].

23. J. P. Bradley, D. E. Brownlee, P. Fraundorf, *Science* **226**, 1432 (1984); K. Thiel, J. P. Bradley, R. Spohr, *Nucl. Tracks Radiat. Meas.* **19**, 708 (1991).

24. R. L. Fleischer, P. B. Price, R. M. Walker, *Nuclear Tracks in Solids: Principles and Applications* (Univ. of California Press, Berkeley, 1975).

25. J. Bibring et al., *Science* **175**, 753 (1972); M. Maurette and P. B. Price, *ibid.* **187**, 121 (1975).

26. H. Y. McSween, *Geochim. Cosmochim. Acta* **47**, 1777 (1977).

27. A. O. Nier and D. J. Schlutter, *Meteoritics* **28**, 675 (1993).

28. J. Taftø and J. Zhu, *Ultramicroscopy* **9**, 349 (1982); P. E. Batson, *Nature* **366**, 727 (1993); D. A. Muller, Y. Tzou, R. Raj, J. Silcox, *ibid.*, p. 725.

29. J. C. Pivin, *J. Mater. Sci.* **18**, 1267 (1983).

30. D. M. Paruso, W. A. Cassidy, B. W. Hapke *Proc. Lunar Planet. Sci. Conf.* **9**, 1711 (1978); M. F. Hochella, J. R. Lindsay, V. G. Mossotti, C. M. Eggleston, *Am. Mineral.* **73**, 1449 (1988); R. Kelly, I. Bertóti, A. Miotello, *Nucl. Instrum. Methods Phys. Res. B* **80/81**, 1154 (1993).

31. P. Sigmund, *J. Appl. Phys.* **50**, 7261 (1979).

32. L. P. Keller and D. S. McKay, *Science* **261**, 1305 (1993); *ibid.* **264**, 1780 (1994); T. J. Bernatowicz, R. H. Nichols, C. M. Hohenberg, *Lunar Planet. Sci. Conf. XXIV*, 105 (1994); T. J. Bernatowicz, R. H. Nichols Jr., C. M. Hohenberg, M. Maurette, *Science* **264**, 1779 (1994); B. Hapke, W. Cassidy, E. Wells, *ibid.*, p. 1779.

33. J. F. Kerridge and I. R. Kaplan, *Proc. Lunar Planet. Sci. Conf.* **9**, 1687 (1978); B. Hapke, W. Cassidy, E. Wells, *Moon* **13**, 339 (1975); J. F. Kerridge, *Lunar Planet. Sci. Conf. XXI*, 301 (1991).

34. F. Liebau, *Structural Chemistry of Silicates: Structure, Bonding, and Classification* (Springer-Verlag, New York, 1985).

35. L. A. Grunes, R. D. Leapman, C. N. Wilker, R. Hoffmann, A. B. Kunz, *Phys. Rev. B* **25**, 7157 (1982).

36. M. T. Otten and P. R. Buseck, *Phys. Chem. Minerals* **14**, 45 (1987).

37. J. P. Bibring et al., *Earth Planet. Sci. Lett.* **22**, 205 (1974).

38. D. E. Brownlee, M. M. Wheelock, S. Temple, J. P. Bradley, J. Kissel, *Lunar Planet. Sci. Conf. XVIII*, 133 (1987); M. E. Lawler, D. E. Brownlee, S. Temple, M. M. Wheelock, *Icarus* **80**, 225 (1989).

39. J. A. Nuth and B. Donn, *J. Geophys. Res.* **88**, A847 (1983).

40. D. K. Aitken, P. F. Roche, C. H. Smith, S. D. James, J. H. Hough, *Mon. Not. R. Astron. Soc.* **230**, 629 (1988); A. G. G. M. Tielens, in *From Miras to Planetary Nebulae: Which Path for Stellar Evolution*, M. O. Mennessier, Ed. (Editions Frontiers, Gif sur Yvette, 1990), p. 186.

41. J. C. Dran et al., *Nucl. Instrum. Methods B* **1**, 557 (1984).

42. This research was supported by NASA (contract NASW 4832). I thank T. VanderWood and R. Wilson for technical assistance and D. Brownlee and T. Bernatowicz, D. Burnett, L. Keller, M. Maurette, and K. Thiel for critical discussions. I thank D. Brownlee for supplying the image in Fig. 1A.

24 January 1994; accepted 24 June 1994

Impact Crater Densities on Volcanoes and Coronae on Venus: Implications for Volcanic Resurfacing

Noriyuki Namiki* and Sean C. Solomon

The density of impact craters on large volcanoes on Venus is half the average crater density for the planet. The crater density on some classes of coronae is not significantly different from the global average density, but coronae with extensive associated volcanic deposits have lower crater densities. These results are inconsistent with both single-age and steady-state models for global resurfacing and suggest that volcanoes and coronae with associated volcanism have been active on Venus over the last 500 million years.

Volcanic features are widely distributed over the surface of Venus (1), and their ages provide critical information on the magmatic budget of the planet. However, the generally low density of impact craters on Venus, a result of atmospheric shielding (2, 3), has prevented a comparison of crater retention ages among small regions (4) and contributes to the controversy over whether a catastrophic (2) or an equilibrium model (3) better describes the global resurfacing history. The spatial diversity of the crater distribution has nonetheless been addressed by grouping areas by latitude or longitude (2), radar cross section (3), elevation (5), or terrain type (6). Following this practice, we have integrated the areas and cratering records for large volcanoes and for coronae

(7) on Venus, and we assess here the implications of the results for volcanism and global resurfacing.

We made use of a database of 841 impact craters classified according to the extent of tectonic deformation and of embayment or partial covering by volcanic material (5, 8). A database for 175 volcanoes at least 50 km in diameter (9), compiled from Magellan images and a published map (1), includes radius and relief of the topographic edifice and the dimensions of the radial flow apron. A database for 358 coronae (10) includes a classification by feature type and extent of interior volcanism. There are 51 features listed in both the volcano and corona databases, because in many coronae there are associated volcanic centers.

For each large volcano, we ascertained from the databases the presence of one or more impact craters on the edifice or flow apron, and from Magellan radar images we determined superposition relations (Fig. 1). We included the edifice and discernible radial flows in calculating the area of each

N. Namiki, Department of Earth, Atmospheric, and Planetary Sciences, Massachusetts Institute of Technology, Cambridge, MA 02139, USA.
S. C. Solomon, Department of Terrestrial Magnetism, Carnegie Institution of Washington, 5241 Broad Branch Road, NW, Washington, DC 20015, USA.

*To whom correspondence should be addressed.

volcano. All embayed craters associated with a large volcano are on plains units exterior to the volcanic edifice. We did not count those embayed craters because of the difficulty of determining whether the impact occurred before or during the period of volcanic activity. Thus, the crater density for large volcanoes measures the average time since major eruptions ceased. We measured the lava flow area for each volcano from Magellan C1-MIDRs and F-MIDRs (11), using meshes of 53 by 53 km² and 18 by 18 km² grids, respectively. The sum of the measured flow areas, the observed total number of impact craters, and the average crater density are given in Table 1. Large volcanoes constitute 5% of the surface of Venus. Because the minimum area necessary to make an independent estimate of crater density on Venus is about 1% of the surface (4), the area covered by large volcanoes is sufficiently large to permit such an estimate.

The distribution of the density of impact craters on large volcanoes with crater diameter is compared with the distribution for the planet as a whole in Fig. 2A. Because we have included in our counts craters whose ejecta deposits barely overlap a volcano flow apron, the effective area of a volcano for a potentially superposed crater is larger than the actual area by an amount that depends on the crater dimensions. We corrected for this difference in the following manner. We determined a flow apron radius for each volcano by finding the circle having the same area as that of the edifice and radial lava flows. Then the effective area was taken equal to that of a circle whose radius is the sum of the radius of the flow apron, the radius of the crater, and the width of the crater ejecta deposits (12). The ratio of the measured area to the effective area provides a correction to the crater density at a given crater diameter.

The distribution of craters by size, so corrected, can be interpreted in one of two ways. On the basis of the similarity of densities of impact craters larger than 16 km in diameter on large volcanoes and on the planet as a whole, it might be argued that the surfaces of large volcanoes are the same average age as the planet overall (6), but that smaller craters have been preferentially removed by volcanic infilling. This explanation is problematic, however, when the fact that we have excluded embayed craters in the counts is taken into account. It is hard to conceive of a mechanism that would remove small craters but that would fail to embay the larger craters included in the counts. The second interpretation acknowledges the large uncertainties in the densities of the largest craters and makes use of the entire

distribution as an integrated measure of crater density. Although the distribution of impact craters on large volcanoes can be distinguished from that for the entire planet, the hypothesis that the two distributions differ by a scalar multiple cannot be rejected at high confidence (13).

The corrected average density of impact craters of all diameters on large volcanoes, at $(0.9 \pm 0.2) \times 10^{-6} \text{ km}^{-2}$, is significantly less than the global average of $(2.0 \pm 0.1) \times 10^{-6} \text{ km}^{-2}$ (2, 3). Further, the fraction of craters associated with large volcanoes embayed by volcanic deposits (33%) is much higher than the global fraction of embayed craters for the planet as a whole (6.5%). Thus, the surfaces of large volcanoes are, on average, younger than the mean age for the planet of about 500 million years (My) (2, 3, 14). This result is consistent with the inference, but does not require, that large volcanoes as a class have relatively young ages. The age of initiation of volcanic activity at each center is, of course, greater than the age of the present volcano surface. On Earth, activity at intraplate hot spots and continental flood basalt provinces can last between several million years and 100 My (15, 16). The lifetimes of volcanoes on Venus, however, are poorly constrained. There is also a possibil-

ity that the morphology of some old volcanoes may be sufficiently different from that of younger volcanoes that the oldest volcanoes have not yet been identified as volcanic centers. If so, the crater densities obtained here are appropriate only to the youngest fraction of centers of volcanic construction.

For a global average surface age of 500 My (2, 3, 14), then from the total area of identified large volcanoes and associated radial flows we may infer an average rate of resurfacing by large volcanoes since that time of $0.05 \text{ km}^2 \text{ year}^{-1}$. This figure underestimates the overall volcanic resurfacing rate, of course, because many other types of volcanic landforms occur on Venus (1). If we assume that all embayed craters can be attributed to volcanic activity and that the density of partially embayed craters is a constant for all volcanic deposits younger than the mean crater retention age, then the area of volcanic flows capable of manifesting an embayment relation in Magellan images is estimated to be $1.0 \times 10^8 \text{ km}^2$, or equivalently 22% of the surface, and the global volcanic resurfacing rate over the last 500 My is calculated as $0.2 \text{ km}^2 \text{ year}^{-1}$.

We may convert these areal resurfacing rates to volumetric fluxes by noting that large craters are more resistant to volcanic

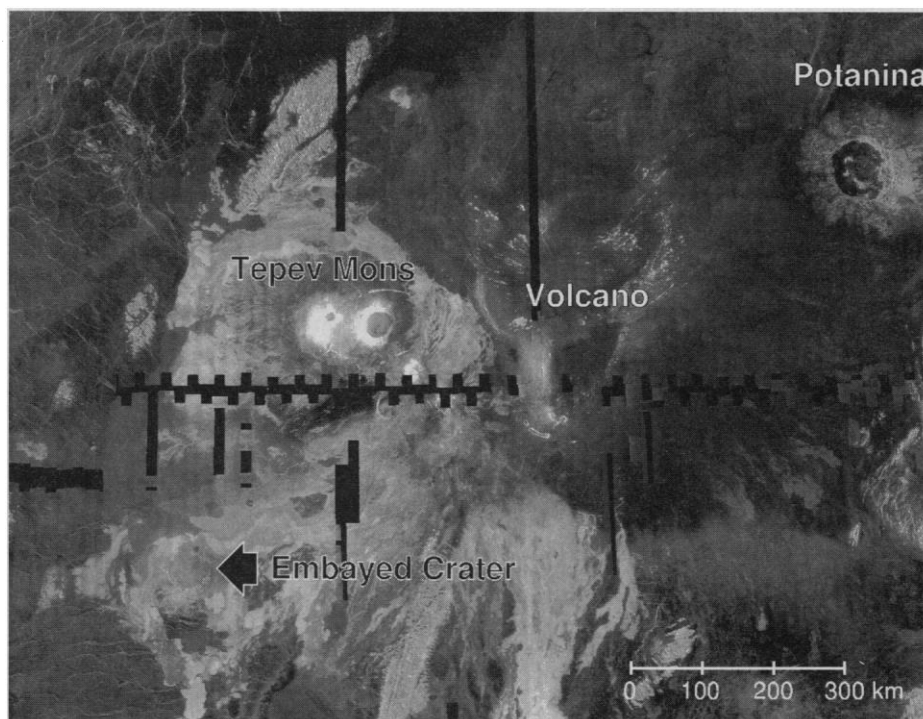


Fig. 1. Magellan radar image illustrating volcano-crater superposition relations in southern Bell Regio. The image is centered at 29°N and 47°E and is 1300 km wide. The impact crater Potanina (90 km in diameter) in the upper right portion of the image overlies radar-dark lava flows emanating from an unnamed volcano near the center of the image. In the southwest portion of the image, radar-bright flows nearly completely embay a 60-km-diameter impact crater. This and the following images are in sinusoidal equal-area projection: north is up; the radar illumination is from the left; and radar cross sections have been linearly stretched to enhance contrast. Black areas are data gaps.

embayment than small craters and should therefore have a higher ratio of partially embayed craters. In Fig. 3 we show the fraction of embayed craters versus crater diameter (5, 8). We suggest that the distinct increase in this fraction at a diameter near 30 km occurs because craters larger than this size tend to survive volcanic embayment. The depth and the rim height of a 30-km-diameter crater on Venus inferred from Magellan radar image measurements (12) are about 1.6 km and 0.5 to 0.8 km, respectively. We thus take 2 km as a conservative upper bound on the average thickness of embaying flow units. This value is comparable to average thickness of terrestrial continental flood basalt occurrences of 0.65 to 5 km (15). From the above estimate of the total area of lava flows capable of embaying craters, upper bounds on the volume of such flow units and the extrusive component of the magmatic flux over the last 500 My are $2.0 \times 10^8 \text{ km}^3$ and $0.4 \text{ km}^3 \text{ year}^{-1}$, respectively. The latter bound is consistent with estimates of the volcanic

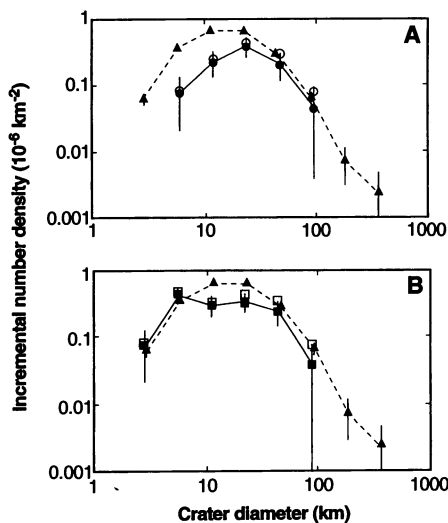


Fig. 2. Distribution of impact craters by crater diameter. Craters are binned into increments at intervals of a factor of 2 in diameter (the full crater density is the sum of these incremental densities). (A) Crater density on large volcanoes (circles). (B) Crater density on coronae (squares). Corrected densities are shown by filled symbols. The overall distribution for the planet is also shown (triangles). Error bars are indicated for the corrected densities and the global distribution (27).

flux obtained from two-dimensional and three-dimensional Monte Carlo resurfacing models (0.01 to 0.15 and $0.37 \text{ km}^3 \text{ year}^{-1}$, respectively) constrained to fit the observed global crater distribution and the fraction of partially embayed craters (17).

Magma reaching the surface as volcanic eruptions, of course, represents only a portion of the total amount of magma generated. A variety of intrusive volcanic landforms has been observed on Venus (1), and there is more intrusive than extrusive magmatism on Earth (18). However, little is known about the ratio of intrusive to extrusive magmatism on Venus. Such a ratio is likely controlled by the brittle strength of the crust and the ability of magma to propagate in dikes and sills (19). Estimates of the fracture toughness, or the resistance to fracture growth, and the maximum distance of propagation of shallow crustal magma for Venus are not significantly different from terrestrial values (19, 20). Therefore, as a conservatively large estimate of the ratio of intrusive to extrusive magmatism on Venus, we adopt the value 17, the maximum ratio documented on Earth (18). Upper bounds on the total volume of magmatic material and the magmatic flux over the last 500 My are then $3.6 \times 10^9 \text{ km}^3$ and $7.2 \text{ km}^3 \text{ year}^{-1}$, respectively. The latter figure is within the range in estimates for the current rate of volcanism and near-surface magmatism on Venus (0.4 to $11 \text{ km}^3 \text{ year}^{-1}$) inferred from the

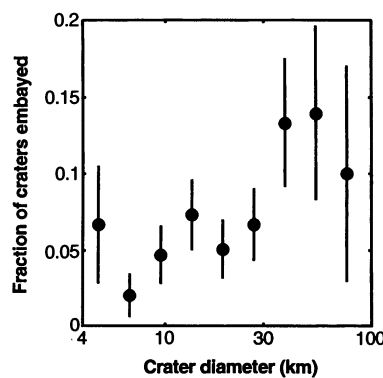


Fig. 3. Fraction of impact craters on Venus embayed by exterior lava flows versus crater diameter (27). Data are from (5) and (8).

rate of reaction of atmospheric SO_2 and surface carbonates (21).

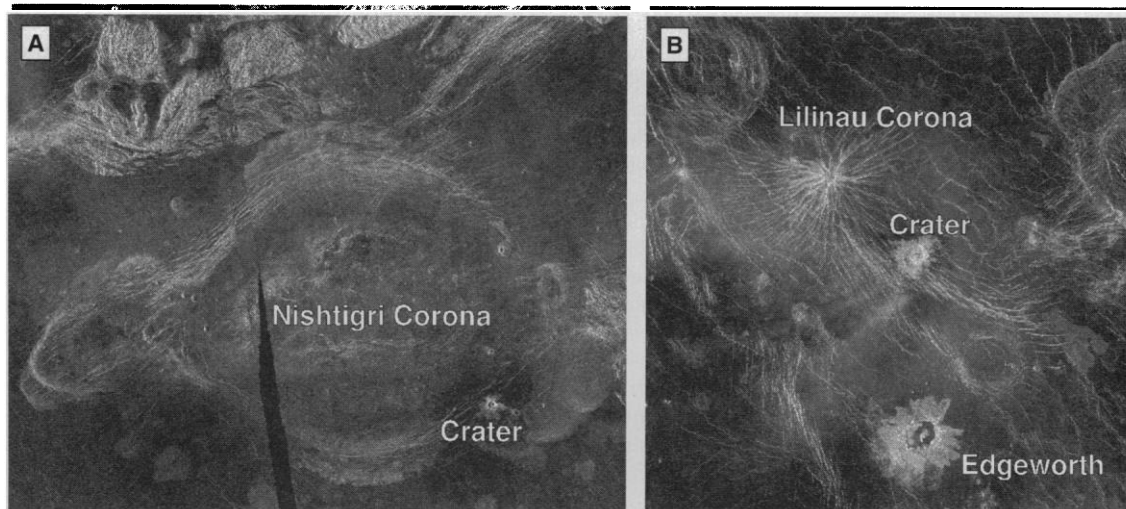
For coronae, we determined the impact crater density within corona interiors (Fig. 4); for most coronae, the interior was taken to be the outer radius of the tectonic annulus. The area of each corona was taken from the dimensions given in the corona database (10). The crater density on coronae and its distribution with crater diameter were corrected for effective area in the same manner as for craters on large volcanoes (Fig. 2B and Table 1). The density of craters 8 km and larger in diameter is somewhat less than average for the planet, whereas the density of craters less than 8 km in diameter is somewhat greater than average. The small craters on coronae are not secondary craters, because no candidate primary craters are sufficiently near. Nor is the greater density of small craters due to a greater fractional coverage of full-resolution images of coronae than for the planet as a whole. Because of the small numbers of craters in each size range, we prefer, as with large volcanoes, to use the entire distribution of craters, rather than only a portion of the distribution, to assess crater density (22). Artemis, about 2200 km in diameter and the largest corona on Venus (10), occupies nearly 15% of the total area of coronae and includes five craters. The crater density for coronae with Artemis excluded, however, is unchanged from that for all coronae (Table 1). Overall, the corrected average density of impact craters on coronae, at $(1.4 \pm 0.2) \times 10^{-6} \text{ km}^{-2}$, is midway between that for large volcanoes and the global average (Table 1). The significance of this result is illuminated by a consideration of geological evidence for corona evolution.

A general sequence of corona development has been postulated from geological studies of Venera 15 and Venera 16 and Magellan images of individual coronae (10, 23). This evolutionary sequence consists of three stages (10). The first stage is characterized by uplift, interior deformation including extensive radial extensional faulting, and volcanic construction. In the second stage, formation of the tectonic annulus and trough occurs, along with continued volcanism. In the last stage coronae are no longer foci for activity but may be partially embayed by regional volcanic deposits or faulted during regional tectonic deformation (10, 23). On the basis of this scenario, coronae have been classified into five groups according to feature type, extent of associated volcanism, and extent of regional embayment by smooth plains material (10). The first group (termed radial, radial-concentric, and volcanic coronae) are held to correspond to the earliest stage of corona for-

Table 1. Summary of crater counts on large volcanoes and coronae (27–29).

Feature type	Number of craters			Area (10^6 km^2)	Uncorrected (corrected) crater density (10^{-6} km^{-2})
	Unmodified	Embayed	Deformed		
Volcanoes	26	14	4	25	1.0 ± 0.2 (0.9 ± 0.2)
Coronae	33	3	9	27	1.7 ± 0.2 (1.4 ± 0.2)
(Excluding Artemis)	32	1	7	23	1.7 ± 0.3 (1.4 ± 0.2)

Fig. 4. Magellan images of coronae and associated impact craters. **(A)** Nishtigri Corona, centered at 24.5°S and 72°E, has a maximum width of 275 km. The image is 500 km wide. The corona has been assigned to volcanic category 2 (10). A deformed impact crater (6 km in diameter) is visible on the tectonic annulus in the southeastern quadrant. **(B)** Lilinau Corona, approximately 200 km in width. The image is centered at 33.5°N and 22.5°E and is 400 km wide. This is an example of a radial corona (10), which consists of predominantly radial tectonic structures and generally lacks an annulus of concentrated deformation. The "interior" of such a feature is less clear cut than for traditional coronae but for our study is taken from the radial dimensions. Two unmodified impact craters (18 and 29



km in diameter) are visible on the image. The crater nearest the corona center is counted in our statistics.

mation. The second to fourth groups (termed categories 1, 2, and 3) are distinguished by an increasing intensity of associated interior volcanism (10) and are held to represent successive evolution within the second stage of corona development. The last group (termed categories 2r and 3r) are older coronae no longer individually active.

The average crater density for each corona group is shown in Fig. 5. Although the small numbers of craters prevent quantitative discussion with high confidence, differences in crater density among corona groups can be recognized (24). The first (radial-volcanic) and second (category 1) groups have a combined crater density indistinguishable from the global average and, by implication, are comparable in average age. It is possible that some of the craters on such coronae predate the tectonic development of the corona structures. Older craters are likely to have been deformed during corona evolution. Three craters among 13 craters on the first and second groups of coronae are classified as tectonically deformed; the density of remaining craters is $(1.4 \pm 0.5) \times 10^{-6} \text{ km}^{-2}$ for these two corona groups. This figure should be regarded as a lower bound, however, because the deformed craters may have formed during the interval of corona evolution or their deformation may have occurred as a result of regional tectonic modification after corona development. Regionally embayed coronae (categories 2r and 3r) also have a crater density similar to the global average. Only coronae with extensive associated volcanic deposits (categories 2 and 3) have crater densities clearly less than the average value for the planet.

The crater densities in Fig. 5 are not those expected if coronae are distributed in age and if all coronae evolve from the radial or volcanic stages through the stages represented by corona categories 1 through 3. If all coronae evolve through the full postulated sequence of evolutionary stages, then those in early phases of evolution should be younger and thus have a lower crater density than those in later phases. The crater densities instead suggest that many coronae represent features that for the most part ceased to develop after a time near the global mean age of the surface. The lower crater densities of category 2 and category 3 coronae, however, indicate that volcanic deposits in these features are considerably younger. This result is consistent with the observation that volcanism tends to become more concentrated within corona interiors as coronae evolve (25).

The crater densities obtained in this study provide a strong constraint on the history of resurfacing on Venus, one of the most fundamental questions raised by Magellan radar observations (2, 3). If the surface of Venus were uniform in age or if crater production and resurfacing were in equilibrium, then the crater density on volcanoes should equal the global average density regardless of the mix of global resurfacing mechanisms or the rate of volcanic activity (26). That crater densities on large volcanoes and on some coronae are significantly lower than the global average is inconsistent with both of these end-member models. Our results suggest that large volcanoes and coronae with voluminous associated volcanic deposits have been magmatically active during the past 500 My. Further, a crater density about half the global average is consistent with an age distribution for such features that is approximately uniform over that

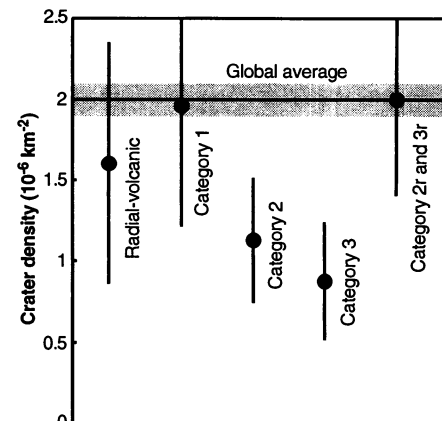


Fig. 5. Crater densities on coronae by corona class (10, 27). Crater density is corrected for effective area as described in the text.

time interval. About 20% of the surface of Venus has been volcanically resurfaced during that time.

REFERENCES AND NOTES

1. J. W. Head, L. S. Crumpler, J. C. Aubele, J. E. Guest, R. S. Saunders, *J. Geophys. Res.* **97**, 13153 (1992).
2. G. G. Schaber *et al.*, *ibid.*, p. 13257.
3. R. J. Phillips *et al.*, *ibid.*, p. 15921.
4. J. J. Plaut and R. E. Arvidson, *ibid.* **93**, 15339 (1988).
5. R. R. Herrick and R. J. Phillips, *Icarus*, in press.
6. M. A. Ivanov and A. T. Basilevsky, *Geophys. Res. Lett.* **20**, 2579 (1993).
7. Coronae are circular to ovate volcanotectonic structures 60 to more than 2000 km in diameter generally distinguished by an annulus of closely spaced deformational features.
8. The original database includes 838 craters; we added three craters on the basis of recently distributed Magellan images. An independently compiled database (2) lists impact craters but does not classify them by extent of tectonic deformation or exterior embayment. Using the latter database increases the impact crater density on volcanoes and coronae by 14 and 13%, respectively, principally by the addition of craters less than 15 km in diameter.

9. P. J. McGovern, C. B. Siren, S. C. Solomon, unpublished material.

10. E. R. Stofan *et al.*, *J. Geophys. Res.* **97**, 13347 (1992). We modified the original database by removing four entries and adjusting the maximum widths of five features on the basis of Magellan images.

11. G. H. Pettengill, P. G. Ford, W. T. K. Johnson, R. K. Raney, L. A. Soderblom, *Science* **252**, 260 (1991). C1- and F-MIDRs are compressed-once and full-resolution Magellan image data records, respectively. Where the edges of lava flows are not clear in standard images, we applied high-pass and median filtering to measure flow area.

12. V. L. Sharpton, *Eos* **73** (fall meeting suppl.), 331 (1992). We have assumed an ejecta width that is 0.4 of the crater diameter.

13. On the basis of a χ^2 test, the probability that the two distributions are identical is 0.02%; the probability that the two are the same except for a scaling factor is 74%.

14. The average crater retention age of the surface on Venus has been estimated to lie between 210 and 720 My (2) and between 400 and 800 My (3). We take 500 My as a representative value (2, 3). The areal resurfacing rate and volcanic flux scale inversely with the assumed average age.

15. Basaltic Volcanism Study Project, *Basaltic Volcanism on the Terrestrial Planets* (Pergamon, New York, 1981); P. Cattermole, *Planetary Volcanism* (Horwood, Chichester, U.K., 1989).

16. T. Simkin, *Annu. Rev. Earth Planet. Sci.* **21**, 427 (1993).

17. M. A. Bullock, D. H. Grinspoon, J. W. Head III, *Geophys. Res. Lett.* **19**, 2147 (1993); R. G. Strom, G. G. Schaber, D. D. Dawson, *J. Geophys. Res.* **99**, 10899 (1994).

18. J. A. Crisp, *J. Volcanol. Geotherm. Res.* **20**, 177 (1984); M. F. Coffin and O. Eldholm, *Rev. Geophys.* **32**, 1 (1994).

19. A. M. Rubin and D. D. Pollard, *Volcanism in Hawaii* [*U.S. Geol. Surv. Prof. Pap. 1350* (1987)], p. 1449; E. A. Parfitt, *J. Geophys. Res.* **96**, 10101 (1991); D. McKenzie, J. M. McKenzie, R. S. Saunders, *ibid.* **97**, 15977 (1992).

20. R. A. Schultz, *J. Geophys. Res.* **98**, 10883 (1993). Crustal pore pressure is negligible on Venus because of the absence of water, which may render the crust more resistant to dike propagation than on Earth. However, there is a disagreement of two or more orders of magnitude between experimentally determined and field estimates of fracture toughness (79).

21. B. Fegley Jr. and R. G. Prinn, *Nature* **337**, 55 (1989).

22. A χ^2 test yields a probability of 15% that the distribution of craters on coronae is identical to that for the entire planet; the probability that the two distributions are the same except for a scaling factor is 69%.

23. A. T. Basilevsky *et al.*, *J. Geophys. Res.* **91** (suppl., Proc. Lunar Planet. Sci. Conf. 16th), D399 (1986); E. R. Stofan and J. W. Head, *Icarus* **83**, 216 (1990); A. A. Pronin and E. R. Stofan, *ibid.* **87**, 452 (1990); S. W. Squyres *et al.*, *J. Geophys. Res.* **97**, 13611 (1992).

24. Areas covered by the different corona groups are 2.9, 3.5, 7.6, 6.7, and 5.6×10^6 km² for radial-volcanic, category 1, 2, 3, and 2r-3r coronae, respectively. The areas of the first two groups are too small to permit a reliable estimate of crater density, but the last three groups cover sufficiently large areas (4). On the basis of a χ^2 test, the probability that crater densities in Fig. 5 differ from random variations from an average is 68%.

25. K. M. Roberts and J. W. Head, *Geophys. Res. Lett.* **20**, 1111 (1993).

26. In the end-member equilibrium resurfacing model, the total number of impact craters on the surface, N^G , is described by

$$\frac{dN^G}{dt} = R_p S^G - u_r^G N^G$$

where R_p is the crater production rate per unit area, S^G is the surface area, and u_r^G is the fractional rate of removal of craters by global resurfacing. Similarly, the number of craters on volcanoes, N^V , is described by

$$\frac{dN^V}{dt} = R_p S^V - u_r^G N^V$$

where S^V is the area of volcanoes. Under equilibrium, $dN/dt = 0$. If S^V is constant in time, the crater density on volcanoes is equal to the global average density, R_p/u_r^G .

27. Errors in crater counts are taken to be equal to the square root of the number of craters.

28. On the basis of the crater database (5, 8), 18 large volcanoes have unmodified craters associated with them; 12 large volcanoes have associated embayed craters. These two populations of volcanoes do not overlap. There are four volcanoes which each have an associated deformed crater; two of these craters are also embayed. A total of 143 (82%) of the identified large volcanoes lack any associated impact craters.

29. From (5) and (8), 30 coronae have unmodified craters, three coronae have embayed craters, and eight coronae have deformed craters. Artemis is the only corona displaying associated craters of different classes (one unmodified, two deformed, and two embayed); the three subsets of coronae do not otherwise overlap. A total of 319 coronae (89%) lack any associated impact craters.

30. We thank R. Herrick and P. McGovern for sharing unpublished databases and two anonymous reviewers for constructive comments. This research was supported by the National Aeronautics and Space Administration under grants NAGW-1937 and NAGW-3276.

31 March 1994; accepted 7 July 1994

Discovery of Microwave Emission from Four Nearby Solar-Type G Stars

Manuel Güdel, Jürgen H. M. M. Schmitt, Arnold O. Benz

Radio waves from the sun were detected 50 years ago, but the microwave detection of other single solar-type stars has remained a challenge. Here, the discovery of four solar-type radio stars is reported. These "solar twin" G stars are radio sources up to 3000 times stronger than the quiet sun. The microwaves most likely originate from a large number of relativistic electrons, possibly produced along with coronal heating, a process that is not understood. Two of the stars are younger than the sun and rotate more rapidly; the dynamo process in the stellar interior is therefore presumably more vigorous, resulting in enhanced coronal activity. One of the detections, however, is an old, metal-deficient G dwarf.

The magnetic dynamo in late-type stars results from an interaction between convection and differential rotation, so that coronal activity is expected to be strong in rapidly rotating stars. Consequently, young stars, often having short rotation periods, as well as interacting binaries of late spectral type should be prone to magnetic phenomena. In the radio domain, many red dwarf stars with emission lines in their optical spectra (dMe stars) are known not only as "radio flare stars" but as sources of "quiet" microwave (~ 1 to 10 GHz) emission that is orders of magnitude more luminous than the sun; the latter emission is often ascribed to the gyrosynchrotron mechanism by nonthermal high-energy electrons. Only a few K stars, among them very young objects and rapid rotators, have been detected as strong radio sources (1-4). In a survey of solar-like stars, the dwarf χ^1 Ori was detected as a transient radio source (5), but this G star turned out to be a binary with an M-type companion (6). A very deep integration yielded a weak signal from the slightly evolved F5 IV-V star Procyon, compatible with thermal emission (7), while a

small survey of FV stars revealed no further radio detections (8). A few G stars in RS CVn-type close binaries, forced to rotate rapidly, are known radio emitters (9, 10). Solar-like stars are thought to lose rapidly much of their initial angular momentum early in their lifetime. Therefore, nonthermal magnetic microwave activity of single stars is expected to decline rapidly with age and to become undetectable with present-day instruments at spectral types earlier than K. The sun, a middle-aged ($\sim 5 \times 10^9$ years) G2V single star, does not emit considerable continuous, nonthermal microwave radiation, and its free-free emission would be difficult to detect even at the distance of the nearest stars ($\sim 30 \mu\text{Jy}$ at 1.3 pc).

The apparent dichotomy between strong stellar and weak solar microwave emission raises a number of questions: Is the prominent coronal activity of the coolest and the youngest stars intrinsically different from what we observe on the sun? Are coronae of the truly solar-type G dwarfs inherently much less prone to continuous or frequent acceleration of energetic particles? To address these questions and possibly link microwave activity on late-type stars to the solar analog (the "solar-stellar connection"), we conducted a deep microwave survey of 15 selected G stars with the Very Large Array (VLA) (11) at its sensitive X band (8.5 GHz) in

M. Güdel, Joint Institute for Laboratory Astrophysics, University of Colorado and National Institute of Standards and Technology, Boulder, CO 80309-0440, USA, and Paul Scherrer Institut, 5232 Villigen PSI, Switzerland. J. H. M. M. Schmitt, Max Planck-Institut für Extraterrestrische Physik, 85740 Garching, Germany. A. O. Benz, Institut für Astronomie, ETH Zentrum, 8092 Zürich, Switzerland.